IRANIAN JOURNAL OF PHYSICS RESEARCH

Iranian Journal of Physics Research, Vol. 6, No. 3, 2006

Electron-hole asymmetry in high-T_c cuprates from theoretical viewpoints

T Tohyama

Yukawa Institute for Theoretical Physics, Kyoto University, Kyoto
E-mail: tohyama@imr.tohoku.ac.jp

(Received 28 July 2006; accepted 30 September 2006)

Abstract

Asymmetric features of various physical quantities in the normal and superconducting states between hole- and electron-doped cuprate high-temperature superconductors have been an issue of debate for a long time. Their exploration is very important for the understanding not only of the mechanism of high-T_c superconductivity but also of the nature of doped-Mott insulators. Presented in this review is the present status of theoretical understanding of the electronic states in hole- and electron-doped high- T_c cuprates as well as the origin of the electron-hole asymmetry of the electronic states. In particular, it is shown that numerically exact diagonalization calculations for small clusters in a *t-J* model with long-range hoppings, t' and t'' nicely reproduce the electron-hole asymmetry observed experimentally in various quantities and thus make it possible to extract the physical origin of the asymmetry. These results give a deep insight on the asymmetric behaviors in hole- and electron-doped high-T_c cuprates and on the nature of doped Mott insulators.

Keywords: electron-hole asymmetry, t-t'-t''-J model, doped Mott insulator

1. Introduction

In 1986, Bednorz and Müller reported high-T_c superconductivity in a copper oxide La-Ba-Cu-O [1]. The confirmation of the superconductivity by Uchida *et al*. [2] triggered a subsequent feverish activity. Even now, twenty years after the discovery, we do not have a final answer for the mechanism of superconductivity in spite of intensive studies by many researchers around the world. However, it is also true that there have been much progresses toward the understanding of the unusual properties of the normal and superconducting states of the high-T_c cuprates.

The most dramatic features of high-T_c cuprates are that the superconductivity emerges as a consequence of carrier doping into a two-dimensional (2D) Mott insulator composed of CuO_2 planes and that the superconductivity exists in a certain finite range of carrier density. This naturally suggests the importance of strong electron correlations in high-T_c superconductivity. Soon after this discovery, the importance of strong electron correlation in the CuO_2 plane was pointed out [3]. These correlations are manifest by the fact that the CuO_2 planes without extra carriers are a Mott insulator. The emerging physics which has to be elucidated is therefore that of a carrier-doped Mott insulator. Although many authors have discussed the electronic properties in 2D cuprates from the view point of strong electron correlation, the problems still remain controversial.

The carrier introduced into the cuprates is either an electron or a hole. Although the symmetry of superconducting order parameter is common with *d*-wave in both cases [4,5], the phase diagrams exhibit asymmetric behaviors between the electron and hole carriers. Figure 1 shows a schematic phase diagram for high-T_c cuprates, where x represents carrier concentration in the CuO_2 plane for both hole and electron dopings. (For instance, $x = 0.1$ means that on average 0.1 holes (electrons) are found on the CuO_2 unit cell.) At $x = 0$ (undoping), the system is a Mott insulator with antiferromagnetic (AF) order below $T \sim 300$ K.

Upon hole doping, the system begins to show metallic behavior in the resistivity at high temperatures [6], and the AF order is rapidly destroyed so that the AF phase is confined to very small region. In the region between the AF phase and superconducting phase, a disordered phase showing a spin glass behavior is observed in $La_{2-x}Sr_xCuO_4$ (LSCO). The superconducting transition temperature (T_c) monotonically increases with hole doping (underdoped region), reaching a maximum at $x \sim 0.15$ (optimal doping). Then, T_c decreases and becomes zero (overdoped region). This doping dependence forms a dome-like behavior for T_c. The normal state above the pseudogap temperature in the underdoped region and well above T_c in the overdoped

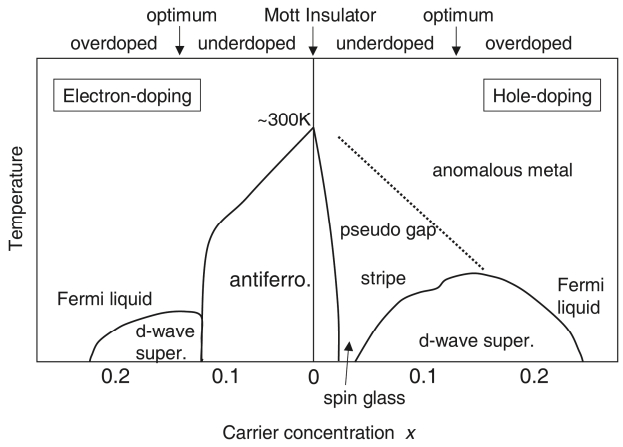

Figure 1. A schematic phase diagram of high- T_c cuprates for both hole and electron dopings. The dotted line is a crossover line between the metallic phase and pseudogap phase.

region exhibits metallic behavior which is different from that of a simple Fermi liquid. For instance, non-T^2 dependence of the resistivity is observed. In the overdoped region, beyond the superconducting dome, a Fermi liquid picture emerges although materials that can reach this region are rare. In the underdoped region above T_c, there is evidence for the existence of a pseudogap. Both spin and charge properties suggest the existence of the pseudogap [7]. In the underdoped region of LSCO, a slight depression of the superconducting dome exists at $x \sim 1/8$, but in a sample of $La_{2-x}Ba_xCuO_4$ (LBCO) T_c completely vanishes at this concentration. At the same time the AF order is recovered. This is called "1/8" anomaly. The physics of the 1/8 anomaly has been unveiled through neutron scattering experiments and Tranquada *et al.* [8] have proposed a novel concept of stripe where one-dimensional charge arrays emerges, accompanying spin domains antiferromagnetically ordered with a shift of spin-ordering phase by π between the charge stripes.

The most prominent difference between hole and electron dopings appears in the AF region near the Mott insulator: In electron-doped systems such as $Nd_{2-x}Ce_xCuO_4$ (NCCO), the AF phase exists over a much larger doping range when compared with hole doping. A difference in magnetic properties is also seen in inelastic neutron scattering experiments: LSCO shows incommensurate spin structures for a wide range of x [9], while in NCCO there is no incommensurate structures but commensurate ones are observed [10]. It is also an important difference that a spin-gap behavior observed in the underdoped region of hole-doped cuprates by the nuclear magnetic resonance experiments is not reported in electron-doped cuprates [11]. It is also prominent that, on the electron-doped side of the phase diagram, there are no reports of a superconducting dome in bulk samples.

Differences in the electronic properties between the hole- and electron-doped cuprates are also observed in other experiments. The optical conductivity obtained from reflectivity measurements exhibits a pseudogap feature at around 0.2 eV in the AF phase of NCCO [12], but there is no such a feature in LSCO with the same carrier concentration [13]. The occurrence of the pseudogap in the optical conductivity is correlated with the strong temperature dependence of the Hall coefficients and a metallic behavior in the c-axis resistivity. From angle-resolved photoemission (ARPES) experiments, it has clearly been observed that hole carriers doped into the parent Mott insulators first enter into the $\mathbf{k} = (\pm\pi/2, \pm\pi/2)$ points in the Brillouin zone and produce a Fermi arc [14,15,16], but electron carriers are accommodated at around $\mathbf{k} = (\pm\pi, 0)$ and $(0, \pm\pi)$ and then the Fermi surface is formed in the superconducting region [17]. The doping dependence of core-level photoemission also shows different behaviors of the chemical potential shift between NCCO and LSCO [18]. These experimental data indicate the difference of the electronic states between hole- and electron-doped cuprates.

In order to clarify the physics behind the asymmetry, we have to understand the electronic states of both types of cuprates and construct proper model that can describe the low-energy excitations of the systems. In fact, there are a plenty of theoretical works related to this issue.

Concerning electron doping, the interplay of the Fermi surface and AF magnetic fructuation with momentum $\mathbf{Q} = (\pi, \pi)$ has been examined by using fluctuation-exchange (FLEX) technique and related ones [19-25]. Those works clearly showed the role of the Fermi surface shape on commensurate magnetic excitations, the suppression of ARPES weight at the Fermi level near crossing points between the Fermi surface and the magnetic Brillouin zone, and nonmonotonic d-wave superconducting gap function observed by ARPES [26]. These works are basically regarded as an approach from overdoped region where correlation effect is relatively weak.

Approaches from Mott insulator for electron doping have mainly been done by using numerical techniques for finite-size clusters and the single-particle spectral functions are compared with those of hole doping [27-32]. In addition to the cluster calculations, a mean-field theory of spin density wave [33] and some analytical approaches such as variational methods [34-36] have been developed to study the spectral functions. All of the calculations have shown that long-range hoppings of electron carriers, in particular, the next-nearest neighbor hopping t', are crucial for coexistence of AF order and the $(\pi, 0)$ electron pocket as well as the presence of a gap along the nodal direction. Therefore, a proper understanding of the effect of t' on electronic and magnetic properties is necessary.

In this review, staring from underlying electronic states of cuprates, we will discuss the role of t' on the asymmetry of hole- and electron-doped cuprates. Taking an approach from the Mott insulating side, we will examine several physical quantities such as the spectral function based on a t-t'-t''-J model and emphasize

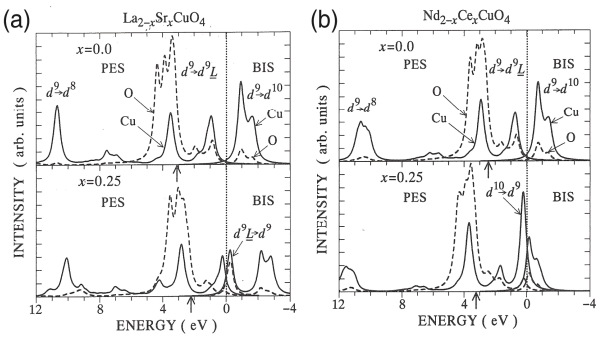

Figure 2. One-particle excitation spectra for Cu3 $d_{x^2-y^2}$ and O2 p_σ orbitals in the middle of the Cu_4O_{13} cluster. (a) $x = 0.0$ and $x = 0.25$ for $La_{2-x}Sr_xCuO_4$ and (b) for $Nd_{2-x}Ce_xCuO_4$. The solid and dashed lines denote Cu3 $d_{x^2-y^2}$ and O2 p_σ spectra, respectively. The zero energy corresponds to the Fermi energy. The vertical arrows denote the positions of the O2 p_σ level. Taken from [39].

the importance of AF correlation in electron doping for the quantities.

This paper is organized as follows. In Sec. 2, we present basic concept of the electronic states of cuprates by introducing the Zhang-Rice singlet state. The t-t'-t''-J model is constructed for both hole- and electron-doped cuprates. Using the t-t'-t''-J model, a simple origin of the stabilization of AF order in the electron doping is discussed based on the approach of doped Mott insulator in Sec. 3. In addition to this, we show several physical quantities that are obtained by the exact diagonalization methods for small clusters. The summary is given in Sec. 4.

2. Underlying electronic states

Insulating cuprates are a charge-transfer-type insulator, where the on-site Coulomb interaction at Cu site is larger than the charge-transfer energy between the Cu and O ions. The most important orbital on oxygen relevant to the electronic states is 2 p_σ orbitals whose wave function has the largest overlap with Cu 3 $d_{x^2-y^2}$ orbitals [37]. These have either 2 p_x or 2 p_y character. Taking 3 d^{10} and 2 p^6 configurations as the vacuums of the system, we introduce a minimum model for the CuO_2 network, including the energy levels of 3 $d_{x^2-y^2}$ and 2 p_σ holes (ε_d and $\varepsilon_d + \Delta$, respectively), the Coulomb repulsion energy of holes on 3 $d_{x^2-y^2}$ (U_d), and on 2 p_σ (U_p), the nearest-neighbor intersite Coulomb energy (U_{pd}), and the hopping energies of holes between nearest-neighbor 3 $d_{x^2-y^2}$ and 2 p_σ orbitals (T_{pd}), and between nearest-neighbor 2 p_σ orbitals (T_{pp}). The model is called the three-band Hubbard model (named for three orbitals in the CuO_2 unit), or the d-p model (named for the inclusion of d and p orbitals), otherwise the Emery model [38]. The Hamiltonian reads

$$H_{dp} = H_\varepsilon + H_U + H_T \tag{1}$$

with

$$H_\varepsilon = \varepsilon_d \sum_{\mathbf{i},\sigma} n^d_{\mathbf{i},\sigma} + (\varepsilon_d + \Delta) \sum_{\mathbf{i},\boldsymbol{\delta},\sigma} n^p_{\mathbf{i}+\boldsymbol{\delta}/2,\sigma}, \tag{2}$$

$$H_U = U_d \sum_{\mathbf{i}} n^d_{\mathbf{i},\uparrow} n^d_{\mathbf{i},\downarrow} + U_p \sum_{\mathbf{i},\boldsymbol{\delta}} n^p_{\mathbf{i}+\boldsymbol{\delta}/2,\uparrow} n^p_{\mathbf{i}+\boldsymbol{\delta}/2,\downarrow} + U_{pd} \sum_{\mathbf{i},\boldsymbol{\delta},\sigma,\sigma'} n^d_{\mathbf{i},\sigma} n^p_{\mathbf{i}+\boldsymbol{\delta}/2,\sigma'}, \tag{3}$$

$$H_T = \sum_{\mathbf{i},\sigma} [T_{pd} d^\dagger_{\mathbf{i},\sigma} \left(p_{\mathbf{i}+\mathbf{y}/2,\sigma} - p_{\mathbf{i}+\mathbf{x}/2,\sigma} - p_{\mathbf{i}-\mathbf{y}/2,\sigma} + p_{\mathbf{i}-\mathbf{x}/2,\sigma} \right) + T_{pp} (p^\dagger_{\mathbf{i}+\mathbf{y}/2,\sigma} p_{\mathbf{i}+\mathbf{x}/2,\sigma} - p^\dagger_{\mathbf{i}-\mathbf{x}/2,\sigma} p_{\mathbf{i}+\mathbf{y}/2,\sigma} + p^\dagger_{\mathbf{i}-\mathbf{y}/2,\sigma} p_{\mathbf{i}-\mathbf{x}/2,\sigma} - p^\dagger_{\mathbf{i}+\mathbf{x}/2,\sigma} p_{\mathbf{i}-\mathbf{y}/2,\sigma}) + \text{h.c.}], \tag{4}$$

where the operator $d_{\mathbf{i},\sigma}$ annihilates holes with spin σ in 3 $d_{x^2-y^2}$ orbital at site $\mathbf{i}$, and $n^d_{\mathbf{i},\sigma} = d^\dagger_{\mathbf{i},\sigma} d_{\mathbf{i},\sigma}$. Here the $p_{\mathbf{i}\pm\mathbf{x}(\mathbf{y})/2,\sigma}$ are the hole annihilation operators for the 2 p_x (2 p_y) orbitals at site $\mathbf{i} \pm \mathbf{x}(\mathbf{y})/2$, $\mathbf{x}$ ($\mathbf{y}$) being the vector connecting neighboring Cu ions along the x (y) directions, and δ in eqs. (3) and (4) is either $\mathbf{x}$ or $\mathbf{y}$ and where $n^p_{\mathbf{i}+\boldsymbol{\delta}/2,\sigma} = p^\dagger_{\mathbf{i}+\boldsymbol{\delta}/2,\sigma} p_{\mathbf{i}+\boldsymbol{\delta}/2,\sigma}$. The signs of the hopping terms in eq. (4) are determined by the phase relations between two orbitals: For hole picture, the sign in front of T_{pd} and T_{pp} becomes + (−) when the phases of the orbitals facing each other are same (different).

The density of states of the d-p model (1) are shown in figure 2. The numerically exact diagonalization method based on the Lanczos technique is used for a Cu_4O_{13} cluster with realistic parameters for LSCO and NCCO [39] (T_{pd} =0.966 (0.840), T_{pp} =0.395 (0.356), and Δ =3.255 (2.394) for LSCO (NCCO), and U_d =8.5, U_p =4.1, and U_{pd} =0 in units of eV). The ground state at $x = 0$ is mainly composed of configurations having one hole at each Cu site, represented by d^9. Spins of the holes interact each other antiferromagnetically with energy J = 0.1-0.16 eV [40]. There are two possible final states from d^9 when we remove an electron: d^9 and $d^9\underline{L}$($\underline{L}$: O2 p hole). The former appears at 10-11 eV in the upper panels of figure 2. The latter makes two structures located at 0.5-2 eV and 2.5-5 eV. The structure at 0.5-2 eV is a split-off state from O2 p main band at 2.5-5 eV, and is called the Zhang-Rice singlet band named after the seminal

work by Zhang and Rice [41]. The final state of an electron-addition spectrum is denoted by d^{10}, which is called the upper Hubbard band. Therefore, the lowest-energy charge excitation from occupied to unoccupied states corresponds to the interband excitation from the Zhang-Rice singlet band to the upper Hubbard band. This represents the Mott gap in the insulating cuprates. We note that, when we map the *d-p* model onto a single band model like the Hubbard or t-J model, we regard the Zhang-Rice singlet band as the lower Hubbard band.

As shown in the lower panels of figure 2, the Fermi level moves to the Zhang-Rice band and the upper Hubbard band upon carrier doping for the La- and Nd-systems, respectively. As a result, new states denoted by $d^9\underline{L} \rightarrow d^9$ and $d^{10} \rightarrow d^9$ appear for the hole and electron dopings, respectively. We note that the shift of the Fermi level is not a simple rigid band shift, but reconstruction of the spectra occurs near the Fermi level. We also note that the spectral weight just above the Fermi level for hole doping and below for electron doping is not the same as the number of doped carriers but larger nearly by twice due to strong electron correlation [42].

Figure 3(a) schematically shows the Zhang-Rice singlet state that is composed of a hole on the $3d_{x^2-y^2}$ orbital and a hole on a linearly combined $2p_\sigma$ orbital. The Zhang-Rice singlet band has a width due to hopping process of the singlet. The singlet can hop not only to nearest-neighbor sites but also to second and third neighbor sites as shown in figure 3(a). The hoppings are denoted as t (nearest neighbor), t' (second neighbor), and t'' (third neighbor). It is important to notice that the magnitude of t' and t'' are predominantly determined by T_{pp}. The d^{10} configuration and its motion are shown in figure 3(b). The configuration behaves similar to the Zhang-Rice singlet, although charges are different. Even in the d^{10} state, there are significant hopping contributions between the second and third neighbors, t' and t'', which are also controlled by T_{pp}. We can map the d-p model onto a single band model according to the procedure given by Zhang and Rice [41], resulting in the t-t'-t''-J model as shown in figure 3(c), where J is the nearest-neighbor exchange interaction between localized spins. The Hamiltonian is given by

$$H = -t\sum_{\mathbf{i},\boldsymbol{\delta},\sigma}\left(\tilde{c}^{\dagger}_{\mathbf{i}+\boldsymbol{\delta},\sigma}\tilde{c}_{\mathbf{i},\sigma}+\tilde{c}^{\dagger}_{\mathbf{i}-\boldsymbol{\delta},\sigma}\tilde{c}_{\mathbf{i},\sigma}\right)- t'\sum_{\mathbf{i},\boldsymbol{\delta}',\sigma}\left(\tilde{c}^{\dagger}_{\mathbf{i}+\boldsymbol{\delta}',\sigma}\tilde{c}_{\mathbf{i},\sigma}+\tilde{c}^{\dagger}_{\mathbf{i}-\boldsymbol{\delta}',\sigma}\tilde{c}_{\mathbf{i},\sigma}\right)- t''\sum_{\mathbf{i},\boldsymbol{\delta}'',\sigma}\left(\tilde{c}^{\dagger}_{\mathbf{i}+\boldsymbol{\delta}'',\sigma}\tilde{c}_{\mathbf{i},\sigma}+\tilde{c}^{\dagger}_{\mathbf{i}-\boldsymbol{\delta}'',\sigma}\tilde{c}_{\mathbf{i},\sigma}\right)+ J\sum_{\mathbf{i},\boldsymbol{\delta}}\mathbf{S}_{\mathbf{i}+\boldsymbol{\delta}}\cdot\mathbf{S}_{\mathbf{i}}\,, \tag{5}$$

where $\boldsymbol{\delta} = \mathbf{x}$ and $\mathbf{y}$, $\boldsymbol{\delta}' = \mathbf{x}+\mathbf{y}$ and $\mathbf{x}-\mathbf{y}$, and $\boldsymbol{\delta}'' = 2\mathbf{x}$ and $2\mathbf{y}$, $\mathbf{x}$ and $\mathbf{y}$ being the unit vectors in the x and y directions, respectively. The operator $\tilde{c}_{\mathbf{i},\sigma} = c_{\mathbf{i},\sigma}(1-n_{\mathbf{i},-\sigma})$ annihilates a localized particle with spin σ at site $\boldsymbol{i}$ with the constraint of no double occupancy, and $S_{\mathbf{i}}$ is the spin operator at site $\boldsymbol{i}$.

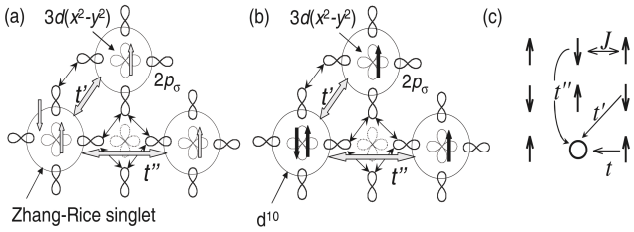

Figure 3. (a) A schematic representation of hoppings of the Zhang-Rice singlet state, t' and t'', in the CuO_2 plane consisting of the $3d\,(x^2-y^2)$ orbital on Cu ion and the $2p_\sigma$ orbital on O ion. The arrows denote spin of a hole. (b) A schematic representation of hoppings of d^{10} configuration created by electron doping. The arrows denote spin of an electron. (c) Interactions of the t-t'-t''-J model. The circle represents the Zhang-Rice singlet state in the original Cu-O model.

The magnitude of t and t' evaluated numerically from d-p clusters [43,44] exhibits small difference between the hole- and electron-doped cuprates in spite of large difference of their electronic states, for instance, $(t,t') = (-0.44, 0.18)$ and $(0.40, -0.10)$ for hole and electron dopings, respectively, in units of eV [43]. This ensures the use of the t-t'-t''-J model for both systems. The magnitude of t'' is usually determined by fitting the Fermi surfaces obtained by the local-density-approximation calculations to those of the tight-binding model. A single-hole dispersion for insulating cuprates is also used for determining t'' [45].

3. Asymmetry of hole- and electron-doped cuprates

Let us start with the single-particle spectral function of the t-t'-t''-J model at half filling ($x = 0$). The spectral function at zero temperature is given by

$$A(\mathbf{k},\omega) = A_{-}(\mathbf{k},\omega) + A_{+}(\mathbf{k},\omega) \tag{6}$$

and

$$A_{\pm}(\mathbf{k},\omega) = \sum_{m,\sigma}\left|\left\langle m\left|a_{\mathbf{k},\sigma}\right|0\right\rangle\right|^2\delta(\omega\mp(E_m-E_0)), \tag{7}$$

where A_- (A_+) is the electron-removal (electron-addition) spectral function, $a_{\mathbf{k},\sigma} = \tilde{c}^{\dagger}_{\mathbf{k},\sigma}$ and $\tilde{c}_{\mathbf{k},\sigma}$ for A_+ and A_-, respectively, $\tilde{c}^{\dagger}_{\mathbf{k}\sigma}$ ($\tilde{c}_{\mathbf{k}\sigma}$) being the creation (annihilation) operator for an electron with momentum $\boldsymbol{k}$ and spin σ. $|m\rangle$ is the eigenstate with the eigenvalue E_m. The chemical potential is set to be zero in energy. To calculate the spectral function, we use numerically exact diagonalization method for a 20-site square lattice and impose twisted boundary conditions instead of standard periodic boundary conditions, in

order to obtain all momenta in the Brillouin zone. Details for calculation have been shown elsewhere [32]. Figure 4 shows the weight map along the high-symmetry lines in the first Brillouin zone. The on-site Coulomb interaction that determines Mott-gap magnitude is set to be $U/|t|=4|t|/J=10$, and $t'/t=-0.25$, $t''/t=0.12$.

The top of the lower Hubbard band is located at $\mathbf{k}=(\pi/2,\pi/2)$. Quasiparticle energies at around $(\pi,0)$ are lower than that of $(\pi/2,\pi/2)$. The spectral weights at around $(\pi,0)$ are suppressed in contrast to the case of the t-J model, where the quasiparticle energies at both $\mathbf{k}=(\pi,0)$ and $(\pi/2,\pi/2)$ are almost degenerate and their weights are similar [45]. On the other hand, the quasiparticle at $(\pi,0)$ in the upper Hubbard band is located at the bottom of the band. Therefore, the charge excitation with minimum energy is from $\mathbf{k}=(\pi/2,\pi/2)$ in the lower Hubbard band to $(\pi,0)$ in the upper Hubbard band. In other words, the Mott gap in the two-dimensional insulating cuprates is an indirect gap. From such an indirect nature, we can expect that doped holes predominantly enter into the $(\pi/2,\pi/2)$ region in heavily underdoping, while the electrons enter into the $(\pi,0)$ region.

We also see in figure 4 that spectral weight at the bottom of the upper Hubbard band ($\mathbf{k}=(\pi,0)$) is the largest among those at other regions. Since spectral weight at half filling is roughly proportional to the product of the weight of the Néel-type configuration in the Heisenberg ground state by that in the single-carrier final state, the large weights at $(\pi,0)$ imply that the Néel-type configuration is dominant in the final states at $(\pi,0)$. Here we note that the $(\pi,0)$ state corresponds to the ground state of one-hole doped t-t'-t''-J model with $t<0$, $t'>0$, and $t''<0$ [45]. The enhancement of the Néel-type configuration among other configurations in the one-hole ground state is caused by the presence of positive t', as explained in the following way. Since t' represents hopping between the same sublattices under AF order, it does not change the spin arrangement of the Néel-type configuration. This means that the magnitude of $-t'$ works as a self energy of the Néel-type configuration. If $-t'$ is negative, the self energy lowers and the Néel-type configuration dominates the one-hole ground state. This results in the enhancement of AF correlation in the ground state. Such negative $-t'$ occurs in the case of electron doping. For hole doping, since $-t'$ is positive, the Néel-type configuration looses its weight in the one-hole ground state and thus AF correlation weakens. Such $-t'$ dependent AF correlation holds for two-hole doped cases [46] and more holes [32].

The asymmetry of spin correlation between hole and electron dopings discussed above can be seen in the dynamical spin correlation function given by

$$S(\mathbf{q},\omega)=\sum_m \left|\langle m|S^z_{\mathbf{q}}|0\rangle\right|^2 \delta\left(\omega-(E_m-E_0)\right) \tag{8}$$

with

$$S^z_{\mathbf{q}}=\frac{1}{\sqrt{N}}\sum_i e^{i\mathbf{q}\cdot\mathbf{R}_i}S^z_i\,, \tag{9}$$

where $S^z_i=(n_{i\uparrow}-n_{i\downarrow})/2$ and N is the total number of lattice site.

Figure 5 shows $S(\mathbf{q},\omega)$ in the $N=20$ t-t'-t''-J lattice [32]. For $x=0.1$ of electron doping, the excitation at $\mathbf{q}=(\pi,\pi)$ exhibits the minimum energy among the momenta defined in the lattice, and has the largest weight. Since the staggered spin correlation indicates the presence of long-range AF order [32], the finite-excitation energy at $\mathbf{q}=(\pi,\pi)$ can be due to the finite-size effect that inevitably causes a discrete energy separation between the ground state and excited states. Away from (π,π), the spectral weights are distributed at the higher-energy region, whose scale is comparable with the spin-wave excitation of the Heisenberg model whose lower-bound edges are denoted by the downward arrows. This again confirms that the ground state is the AF ordered state even in the presence of mobile carriers. With further doping of electrons ($x=0.2$), the (π,π) spectrum looses its weight and the high-energy weights at other momenta shift to the lower-energy side, as expected from the reduction of AF correlation. This doping dependence is qualitatively consistent with recent inelastic neutron scattering measurements for an electron-doped material $Pr_{2-x}Ce_xCuO_4$ [47].

At $x=0.1$ of hole doping, the lowest-energy excitations are not at $\mathbf{q}=(\pi,\pi)$ but at $(\pi,0)$ as shown in Fig. 5(a), although the spectral weight is the highest at (π,π). For $x=0.2$, the (π,π) weight decreases and the weight at $(3\pi/5,4\pi/5)$ shifts to lower energy. These behaviors indicate a tendency toward incommensurate spin correlations reported in hole-doped materials such as LSCO [9] and $YBa_2Cu_3O_{7-\delta}$ [48-50]. At (π,π) for $x=0.1$, we find, from the comparison between the solid and dotted lines, that the introduction of t' and t'' shifts weights to lower-energy side, indicating the shift of AF spin fluctuation toward lower frequencies.

Based on the magnetic properties examined above, we can speculate a schematic energy diagram of the low-energy sectors for the t-t'-t''-J model near half filling as shown in Figure 6. $t'>0$ and $t'<0$ correspond to hole and electron dopings, respectively. Without t' (t-J model), the ground state might be a uniform state of charge with AF short-range correlation but without long-range order. This state may have d-wave superconductivity. Near the ground state, there would be AF ordered state as well as charge-ordered state like a stripe state [8] and a checkerboard state [51-53]. The

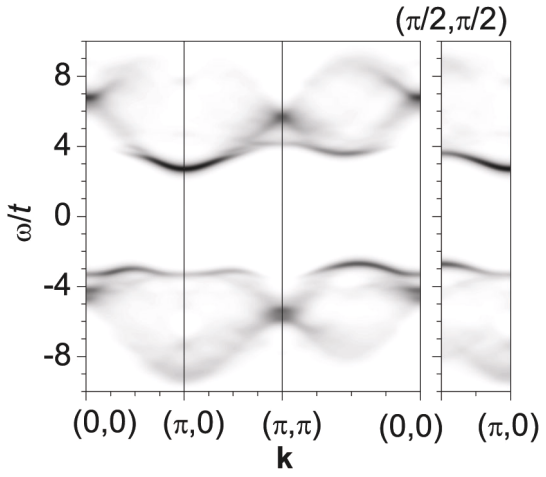

Figure 4. Weight map of the spectral function for a 20-site t - t' - t'' - J model at half filling along the high-symmetry lines. $|t|=1$, $t'/t=-0.25$, $t''/t=0.12$, and $J/|t|=0.4$. Twisted boundary conditions are imposed on the lattice in calculating the final states. For each boundary condition a Lorentzian broadening of $0.2|t|$ is used. The on-site Coulomb interaction that determines the Mott gap magnitude is set to be $U/|t|=4|t|/J=10$. The chemical potential is located at the zero energy. Taken from [32].

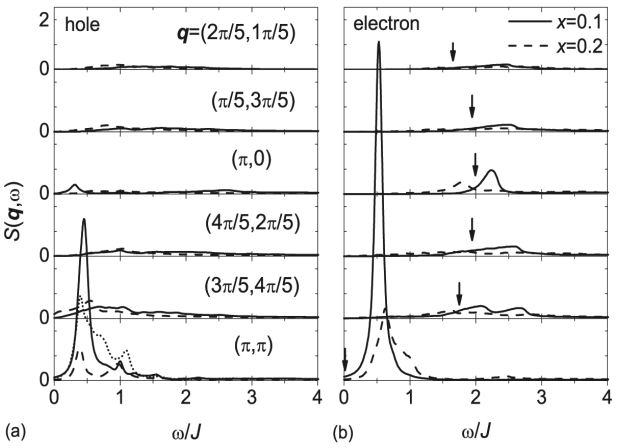

Figure 5. Dynamical spin correlation function $S(\mathbf{q},\omega)$ for a $N=20$ t - t' - t'' - J lattice. (a) Hole doping ($t=1$, $t'=-0.25$, $t''=0.12$, and $J=0.4$) and (b) electron doping ($t=-1$, $t'=0.25$, $t''=-0.12$, and $J=0.4$). Solid and dashed lines represent the data for $x=0.1$ and $x=0.2$, respectively. The dotted line at $\mathbf{q}=(\pi,\pi)$ in (a) represents the data for the t - J model at $x=0.1$. The momenta defined in the lattice are shown in (a). In (b) the edge of the spin-wave excitations in the Heisenberg model ($x=0$) obtained by the linear-spin-wave theory is indicated by the downward arrow for each momentum. Taken from [32].

introduction of t' gives rise to dramatic change of AF state depending on the sign of t' as discussed above. For the electron-doped systems, the AF state becomes the ground state, being consistent experimental observations. On the other hand, the energy of the AF state increases in the hole-doped system and thus the uniform and charge-ordered states would compete each other. In fact, the charge-ordered states have been observed in the hole-doped materials such as $Bi_2Sr_2CaCu_2O_{8+\delta}$ (BSCCO) and $Ca_{2-x}Na_xCuO_2Cl_2$. We would like emphasize that asymmetry of electronic states between hole- and electron-doped cuprates is caused by the presence of t'.

Not only magnetic properties but also spectral functions show remarkable asymmetry between hole- and electron-doped cuprates. Figure 7 shows the asymmetry in the spectral function of a 20-site t - t' - t'' - J lattice [32]. The bold lines in the figure represent a noninteracting tight-binding band with the same hopping amplitudes as $t=1$, $t'/t=-0.25$, and $t''/t=0.12$, which is available for a guide of the band renormalization of the t - t' - t'' - J model.

For a two-hole doped system ($x=0.1$), we find that large spectral weights appear at around $\mathbf{k}=(\pi/2,\pi/2)$ just below and above the Fermi level. We also find that along the $(0,0)$ - (π,π) direction the dispersion exhibits a slight downturn toward $(0,0)$ at $(\pi/2,\pi/2)$. On the other hand, at around $(\pi,0)$ the spectra are located below the Fermi level with small weight and flat dispersion. These behaviors are consistent with the picture that doped holes predominantly occupy the $(\pi/2,\pi/2)$ region in underdoped system, which is expected from the dispersion at half filling as shown in figure 4. The most interesting feature in figure 7(a) is a gapped behavior near the Fermi level along the $(\pi,0)$ - (π,π) direction. This seems to correspond to the pseudogap observed in ARPES experiments for hole-doped high-T_c cuprates [54]. The gap direction is sensitive to the magnitude of t' and t'' [32]. ARPES experiments [55] have shown that the flat band at around $k=(\pi,0)$ is deeper in energy for BSCCO than for LSCO. Since t' and t'' for BSCCO are known to be larger than that for LSCO [45], the experimental data are consistent with the present picture that t' and t'' predominantly control the pseudogap magnitude.

At $x=0.2$ (four holes in the 20-site lattice), the gap becomes less clear than that at $x=0.1$, as shown in figure 7(b). Along the $(0,0)$ - (π,π) direction, the gap feature almost disappears, and a downturn of the dispersion at $(\pi/2,i/2)$, seen at $x=0.1$, vanishes completely. Furthermore, a spectral distribution near the Fermi level along the $(\pi,0)$ - (π,π) direction becomes continuous. We can say that overall behavior gradually approaches to the noninteracting band with increasing the hole concentration.

Figure 7(c) shows $A(\mathbf{k},\omega)$ for a two-electron doped system ($x=0.1$). The spectra are very different from

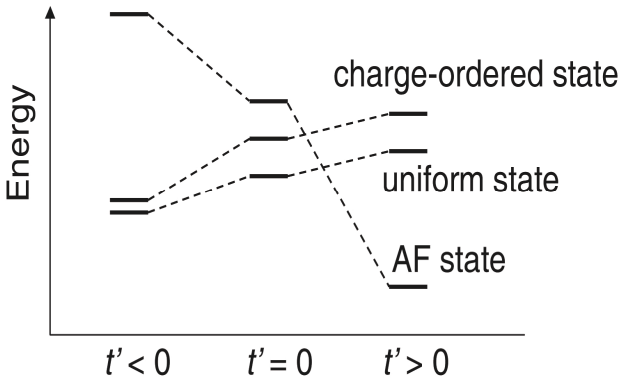

Figure 6. A schematic energy diagram of the ground state and low-energy excited states for the t-t'-t''-J model near half filling. $t'<0$ and $t'>0$ correspond to hole and electron dopings, respectively.

those for hole doping. At around $\mathrm{k}=(\pi,0)$, an electron pocket is seen as expected from the spectral function at half filling (see figure 4). Note that, in order to get such a clear pocket, the presence of AF order is necessary. In fact, strong AF correlation remains in the lattice as explained above. Along the $(0,0)$-(π,π) direction, we find a clear gap in the dispersion. Other calculations of the spectral function for a Hubbard model with long-range hoppings also display gap behaviors consistent with our results as long as U is large [27-31, 33, 36].

The spectral function for a four-electron doped system ($x=0.2$) is exhibited in figure 7(d). The $(\pi,0)$ electron pocket seen at $x=0.1$ almost disappears, although the spectral intensity at around $(\pi,0)$ is still strong enough to show a remnant of the pocket. In contrast, the $(\pi/2,\pi/2)$ gap remains clearly but with smaller gap magnitude. With further doping, the spectra show dispersions similar to a noninteracting system [32].

Let us discuss the origin of the gap along the $(0,0)$-(π,π) direction seen for $x=0.1$ and 0.2 in electron doping. The gap is, of course, the consequence of the presence of t' and t'', because there is no gap at the Fermi level along the nodal direction in the t-J model. Since t' enhances AF correlation as emphasized above, the magnitude of the gap in electron doping seems to be related to the strength of AF correlation. Reflecting the sensitivity to the AF correlation, with increasing J the gap also increases.

An important point to be noticed is that the AF-superconducting transition in electron-doped cuprates may be accompanied by a topology change of the Fermi surface from small to large ones. At the same time, the gap at the Fermi level along the nodal direction is expected to be closed in order for $d_{x^2-y^2}$-wave superconductivity to be induced. However, in the present calculations, the critical electron concentration x_c, where the gap closes, is $x_c\sim 0.3$, which is higher than

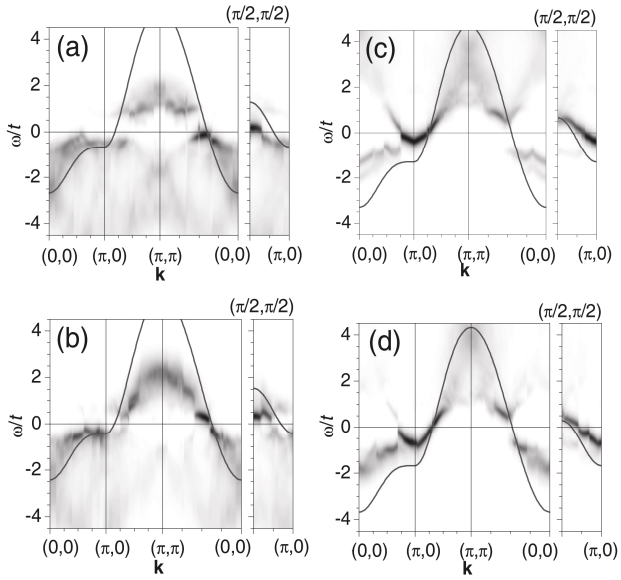

Figure 7. Weight map of the spectral function for a 20-site t-t'-t''-J model. (a) Carrier concentration $x=1-18/20=0.1$ and (b) $x=1-16/20=0.2$ for hole doping ($t=1$, $t'=-0.25$, $t''=0.12$, and $J=0.4$). (c) $x=0.1$ and (d) $x=0.2$ for electron doping ($t=-1$, $t'=0.25$, $t''=-0.12$, and $J=0.4$). The solid curves represent a noninteracting tight-binding band with the same hopping amplitudes. Taken from [32] with modifications.

experimental values of the AF-superconducting transition ($x_c\sim 0.1$-0.15) or a quantum phase transition [56] ($x_c=0.165$). The discrepancy may indicate the presence of additional effects that have not been included in the present t-t'-t''-J model: For instance, (1) the x dependence of the parameter values, which has been incorporated into the studies of a t-t'-t''-U model, [33,27,28,30] and (2) the effect of inhomegeneity, the presence of which has been reported in local probes such as muon-spin relaxation [57] and nuclear magnetic resonance [58,59] experiments. In any case, we may need to clarify the origin of the discrepancy. This still remains as a future issue.

Charge dynamics such as the optical conductivity is also influenced by the asymmetry caused by t'. The real part of the optical conductivity is given by

$$\sigma(\omega)=2\pi e^2 D\,\delta(\omega)+\sigma_{reg}(\omega), \tag{10}$$

where e is the unit of the electric charge ($e>0$), and D is the charge stiffness, which distinguishes an insulator ($D=0$) from a metal ($D\neq 0$) at zero temperature $T=0$ as discussed originally by Kohn [60]. When the electric field is applied along the x direction, the regular part $\sigma_{reg}(\omega)$ at $T=0$ is expressed as

$$\sigma_{reg}(\omega)=\frac{\pi e^2}{N\omega}\sum_m \left|\langle m|j_x|0\rangle\right|^2\delta\left(\omega-(E_m-E_0)\right), \tag{11}$$

where the current operator j_x for the t-t'-t''-J model

is

$$j_x = -it\sum_{\mathbf{i},\sigma}\left(\tilde{c}^{\dagger}_{\mathbf{i}+\mathbf{x},\sigma}\tilde{c}_{\mathbf{i},\sigma} - \tilde{c}^{\dagger}_{\mathbf{i}-\mathbf{x},\sigma}\tilde{c}_{\mathbf{i},\sigma}\right) - it'\sum_{\mathbf{i},\boldsymbol{\delta}',\sigma}\left(\tilde{c}^{\dagger}_{\mathbf{i}+\boldsymbol{\delta}',\sigma}\tilde{c}_{\mathbf{i},\sigma} - \tilde{c}^{\dagger}_{\mathbf{i}-\boldsymbol{\delta}',\sigma}\tilde{c}_{\mathbf{i},\sigma}\right) - i2t''\sum_{\mathbf{i},\sigma}\left(\tilde{c}^{\dagger}_{\mathbf{i}+2\mathbf{x},\sigma}\tilde{c}_{\mathbf{i},\sigma} - \tilde{c}^{\dagger}_{\mathbf{i}-2\mathbf{x},\sigma}\tilde{c}_{\mathbf{i},\sigma}\right). \quad (12)$$

The D satisfies a sum rule:

$$K = -\frac{1}{2N}\langle 0|\tau_{xx}|0\rangle = D + \frac{1}{\pi}\int_0^{\infty}\sigma_{reg}(\omega)d\omega, \quad (13)$$

where the stress-tensor operator τ_{xx} is given by

$$\tau_{xx} = -t\sum_{\mathbf{i},\sigma}\left(\tilde{c}^{\dagger}_{\mathbf{i}+\mathbf{x},\sigma}\tilde{c}_{\mathbf{i},\sigma} + \tilde{c}^{\dagger}_{\mathbf{i}-\mathbf{x},\sigma}\tilde{c}_{\mathbf{i},\sigma}\right) - t'\sum_{\mathbf{i},\delta',\sigma}\left(\tilde{c}^{\dagger}_{\mathbf{i}+\delta',\sigma}\tilde{c}_{\mathbf{i},\sigma} + \tilde{c}^{\dagger}_{\mathbf{i}-\delta',\sigma}\tilde{c}_{\mathbf{i},\sigma}\right) - 2t''\sum_{\mathbf{i},\sigma}\left(\tilde{c}^{\dagger}_{\mathbf{i}+2\mathbf{x},\sigma}\tilde{c}_{\mathbf{i},\sigma} + \tilde{c}^{\dagger}_{\mathbf{i}-2\mathbf{x},\sigma}\tilde{c}_{\mathbf{i},\sigma}\right). \quad (14)$$

Figure 8 shows the dependence of the optical conductivity $\sigma(\omega)$ on the carrier concentration x for the 20-site t-t'-t''-J lattice [32]. At $x = 0.1$, there is a broad-peak structure at around $\omega \sim t$ in addition to the Drude contribution centered at $\omega = 0$ for both the hole and electron dopings. Such a broad-peak structure is known to be incoherent charge excitations accompanied with magnetic excitations [61]. This is physically characterized as an excitation from the AF ground state to an excited state where wrong spin bonds are created by the motion of carriers. As a result of the presence of the broad peak separated from the Drude contribution, a gap-like feature, i.e., a pseudogap, emerges at around $\omega \sim 0.5t$.

For electron doping, it has been discussed [62] that the pseudogap is very sensitive to not only J but also t' and t'': With increasing the absolute values of t'/t and t''/t, the gap increases in energy. Such a pseudogap feature in $\sigma(\omega)$ has been clearly observed in electron-doped NCCO [12]. In figure 8(a), the gap feature is also seen in hole-doped case at $x = 0.1$. Although the gap feature has not been clearly reported in the normal state of hole-doped LSCO, a broad peak can be seen at $\omega \sim 0.5$ eV for $x \le 0.06$ [13]. The calculated broad-peak structure in hole doping probably corresponds to the broad peak observed experimentally.

At $x = 0.2$, a remarkable difference appears between hole and electron dopings in figure 8: A pseudogap remains in electron doping accompanied by a peak at $\omega = 0.7|t|$, while it disappears in hole doping. Since such a gap feature is related to magnetic excitations as discussed above, the difference should reflect the difference of magnetic properties. This clearly demonstrates the fact that charge dynamics is strongly influenced by AF spin correlation. At $x = 0.3$, $\sigma(\omega)$ in

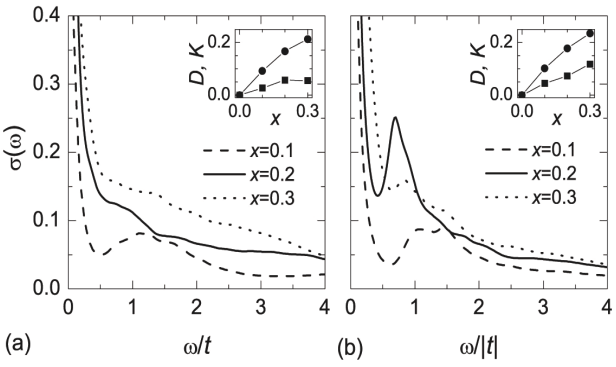

Figure 8. Optical conductivity $\sigma(\omega)$ for a 20-site t-t'-t''-J model. (a) Hole doping ($t = 1$, $t' = -0.25$, $t'' = 0.12$, and $J = 0.4$) and (b) electron doping ($t = -1$, $t' = 0.25$, $t'' = -0.12$, and $J = 0.4$). Dashed, solid, and dotted lines represent the carrier concentration of $x = 0.1$, 0.2, and 0.3, respectively. Delta functions are broadened by a Lorentzian with a width of $0.1|t|$. Insets: The x dependence of the Drude weight D as well as the integrated total weight K. Taken from [32].

electron doping shows similar behaviors to the hole-doped case. This is reasonable because the concentration of $x = 0.3$ is enough to kill AF correlation.

It is also interesting to compare the peak position in $\sigma(\omega)$ with the gap in the single-particle spectral function $A(\mathbf{k},\omega)$ discussed above. In electron doping, the values of the gap $E_{\rm gap}$ at around $\mathbf{k} = (\pi/2, \pi/2)$ are $1.0t$ and $0.74t$ for $x = 0.1$ and 0.2, respectively (see figure 7(a) and (b)). These numbers almost agree to the peak positions in $\sigma(\omega)$ as shown in figure 8(b). Such an agreement indicates that the pseudogap in $\sigma(\omega)$ and the gap in $A(\mathbf{k},\omega)$ in electron doping have the same origin. Needless to say, AF spin correlation is the underlying cause of the gaps.

In the inset of figure 8, the Drude weight D as well as the integrated total weight K defined in eq. (13) is plotted as a function of x. Both the weights increase with x. Comparing the hole and electron dopings, we find that D as well as K is larger in electron doping than in hole doping. Such an enhancement in electron doping, particular for $x \le 0.2$, is a consequence of the interplay between the charge motion and spin background, where the AF spin background makes possible smooth sublattice-charge flows via t' and t'' [62].

4. Summary

In this review, we have examined the role of long-range hoppings on the electron-hole asymmetry of the electronic states in high-T_c cuprates by taking an approach from the Mott insulating side. In order to clarify the role, we concentrated on the doping dependence of magnetic and electronic properties in the hole- and electron-doped cuprates for the t-t'-t''-J

model. We find that a fact that AF spin correlation remains strong in electron doping in contrast to the case of hole doping. This necessarily leads to a remarkable electron-hole asymmetry in the dynamical spin structure factor. The doping dependence of these quantities in electron doping is qualitatively consistent with recent experimental data, indicating the justification for the use of the t - t' - t'' - J model.

We have also uncovered dramatic differences in the single-particle spectral function between hole and electron dopings. In hole doping, the quasiparticle band for $x = 0.1$ is gapless at the Fermi level along the nodal $(0,0)$ - (π,π) direction, but a gapped behavior emerges near the anti-nodal region, being consistent with ARPES data in the underdoped cuprates. It is important to notice that the presence of t' and t'' is essential to the pseudogap. The gap near the anti-nodal region disappears at $x = 0.2$. In contrast, the gap appears near the nodal region in electron doping up to $x = 0.2$. The gap is found to be correlated with the strength of AF correlation, indicating that the gap is magnetically driven. In addition to the gap, an electron pocket is clearly seen at around $(\pi,0)$ for $x = 0.1$.

In the optical conductivity, a pseudogap feature clearly appears in the electron-doped system up to $x = 0.2$. The origin of the gap is attributed to the strong AF correlation in the spin background. In fact, we find that the pseudogap has the same magnitude as that in the spectral function along the nodal direction, confirming the same origin.

Overall agreement between the t - t' - t'' - J results and experiments indicate that an approach from the Mott insulator is suitable for understanding of the physics behind asymmetry between hole- and electron-doped high- T_c cuprates. From this approach, understanding T_c difference between the two systems is one of the most important issues to be solved in near future.

Acknowledgements

I would like to thank S. Maekawa for enlightening discussions and S. A. Jafari for recommending me writing this review. This work was supported by The Next Generation Super Computing project of Nanoscience program, CREST, and Grant-in-Aid for Scientific Research from the Ministry of Education, Culture, Sports, Science and Technology of Japan.

References

1. J G Bednorz and K A Muller, *Z. Physik*, **64** (1986) 189.
2. S Uchida, H Takagi, K Kitazawa and S Tanaka: *Jpn. J. Appl. Phys*. **26** (1987) L1.
3. P W Anderson, *Sience*, **235** (1987) 1196.
4. J R Kirtley, C C Tsuei, J Z Sun, C C Chi, Lock See Yu-Jahnes, A Gupta, M Rupp, and M B Ketchen, *Nature*, **373** (1995) 225.
5. C C Tsuei and J R Kirtley, *Phys. Rev. Lett*. **85** (2000) 182.
6. Y Ando, A N Lavrov, S Komiya, K Segawa and X F Sun, *Phys. Rev. Lett*. **87** (2001) 017001.
7. T Timusk and B Statt, *Rep. Prog. Phys*. **62** (1999) 61.
8. J M Tranquada, B J Sternlieb, J D Axe, Y Nakamura and S Uchida, *Nature*, **375** (1995) 561.
9. K Yamada, C H Lee, K Kurahashi, J Wada, S Wakimoto, S Ueki, H Kimura, Y Endoh, S Hosoya, G Shirane, R J Birgeneau, M Greven, M A Kastner and Y J Kim, *Phys. Rev*. B **57** (1998) 6165.
10. K Yamada, K Kurahashi, T Uefuji, M Fujita, S Park, S-H Lee and Y Endoh, *Phys. Rev. Lett*. **90** (2003) 137004.
11. G-q Zheng, T Sato, Y Kitaoka, M Fujita, K Yamada, *Phys. Rev. Lett*. **90** (2003) 197005.
12. Y Onose, Y Taguchi, K Ishizaka and Y Tokura, *Phys. Rev. Lett*. **87** (2001) 217001; *Phys. Rev*. B (2004) 024504.
13. S Uchida, T Ido, H Takagi, T Arima, Y Tokura and S Tajima, *Phys. Rev*. B **43** (1991) 7942.
14. A Ino, C Kim, M Nakamura, T Yoshida, T Mizokawa, A Fujimori, Z-X Shen, T Kakeshita, H Eisaki and S Uchida, *Phys. Rev*. B **65** (2002) 094504.
15. T Yoshida, X J Zhou, T Sasagawa, W L Yang, P V Bogdanov, A Lanzara, Z Hussain, T Mizokawa, A Fujimori, H Eisaki, Z-X Shen, T Kakeshita and S Uchida, *Phys. Rev. Lett*. **91** (2003) 027001.
16. F Ronning, T Sasagawa, Y Kohsaka, K M Shen, A Damascelli, C Kim, T Yoshida, N P Armitage, D H Lu, D L Feng, L L Miller, H Takagi and Z-X Shen, *Phys. Rev*. B **67** (2003) 165101.
17. N P Armitage, F Ronning, D H Lu, C Kim, A Damascelli, K M Shen, D L Feng, H Eisaki, Z-X Shen, P K Mang, N Kaneko, M Greven, Y Onose, Y Taguchi and Y Tokura, *Phys. Rev. Lett*. **88** (2002) 257001.
18. N Harima, J Matsuno, A Fujimori, Y Onose, Y Taguchi and Y Tokura, *Phys. Rev*. B **64** (2001) 220507.
19. H Kontani, K Kanki and K Ueda, *Phys. Rev*. B **59** 14723 (1999).
20. K Kuroki, R Arita and H Aoki, *Phys. Rev*. B **60** (1999) 9850.
21. H Kondo and T Moriya, *J. Phys. Sco. Jpn*. **68** (1999) 3170.
22. D Manske, I Eremin and K H Bennemann, *Phys. Rev*. B **62** (2000) 13922.
23. Y Yanase and K Yamada, *J. Phys. Soc. Jpn*. **70** (2001) 1659.
24. A Kobayashi, A Tsuruta, T Matsuura and Y Kuroda, *J. Phys. Soc. Jpn*. **71** (2002) 1640.
25. H Yoshimura and D Hirashima, *J. Phys. Soc. Jpn*. **73** (2004) 2057; *ibid.* **74** (2005) 712.
26. H Matsui, K Terashima, T Sato, T Takahashi, M Fujita and K Yamada, *Phys. Rev. Lett*. **95** (2005) 017003.
27. B Kyung, J-S Landry and A-M S Tremblay, *Phys.*

Rev. B **68** (2003) 174502.
28. B Kyung, V Hankevych, A-M Daré and A-MS Tremblay, *Phys. Rev. Lett*. **98** (2004) 147004.
29. B Kyung, et al., *Phys. Rev*. B **73** (2006) 165114.
30. D Sénéchal and A-M S Tremblay, *Phys. Rev. Lett*. **92** (2004) 126401.
31. D Sénéchal, P-L Lavertu, M-A Marois and A-M S Tremblay, *Phys. Rev. Lett*. **94** (2005) 156404.
32. T Tohyama, *Phys. Rev*. B **70** (2004) 174517.
33. C Kusko, R S Markiewicz, M Lindroos and A Bansil, *Phys. Rev*. B **66** (2002) 140513.
34. T K Lee, C-M Ho and N Nagaosa, *Phys. Rev. Lett*. **90** (2003) 067001.
35. Q Yuan, Y Chen, T K Lee and C S Ting, *Phys. Rev*. B **64** (2004) 214523.
36. H Kusunose and T M Rice, *Phys. Rev. Lett*. **91** (2003) 186407.
37. S Maekawa, T Tohyama, S E Barnes, S Ishihara, W Koshibae and G Khaliullin, *Physics of Transition Metal Oxides*, Springer Series in Solid-State Sciences, **144** (2004).
38. V J Emery: *Phys. Rev. Lett*. **58** (1987) 2794.
39. T Tohyama and S Maekawa, *Physica* C **191** (1992) 193.
40. P Bourges, H Casalta, A S Ivanov and D Petitgrand, *Phys. Rev. Lett*. **79** (1997) 4906.
41. F C Zhang and T M Rice: *Phys. Rev*. B **37** (1988) 3759.
42. H Eskes, M B J Meinders and G A Sawatzky, *Phys. Rev. Lett.* **67** (1991) 1035.
43. H Eskes, G A Sawatzky and L F Feiner, *Physica* C **160** (1989) 424.
44. T Tohyama and S Maekawa, *J. Phys. Soc. Jpn*. **59** (1990) 1760.
45. T Tohyama and S Maekawa, *Super. Sci. Tech*. **13** (2000) R17.
46. T Tohyama and S Maekawa, *Phys. Rev*. B **49** (1994) 3596.
47. M Fujita and K Yamada, private communications.
48. S Hayden, H Mook, P Dai, T Perring and F Dogan, *Nature* **429** (2004) 531.
49. V Hinkov, S Pailhès, P Bourges, Y Sidis, A Ivanov, A Kulakov, C T Lin, D P Chen, C Bernhard and B Keimer, *Nature* **430** (2004) 650.
50. D Reznik, P Bourges, L Pintschovius, Y Endoh, Y Sidis, T Matsui and S Tajima, *Phys. Rev. Lett*. **93** (2004) 207003.
51. J E Hoffman, E W Hudson, K M Lang, V Madhavan, H Eisaki, S Uchida and J C Davis, *Science* **295** (2002) 466.
52. M Vershinin, S Misra, S Ono, Y Abe, Y Ando and A Yazdani, *Science* **303** (2004) 1995.
53. T Hanaguri, C Lupien, Y Kohsaka, D-H Lee, M Azuma, M Takamo, H Takagi and J C Davis, *Nature* **430** (2004) 1001.
54. A Damascelli, Z Hussain and Z-X Shen, *Rev. Mod. Phys*. **75** (2003) 473, and references therein.
55. K Tanaka, T Yoshida, A Fujimori, D H Lu, Z-X Shen, X-J Zhou, H Eisaki, Z Hussain, S Uchida, Y Aiura, K Ono, T Sugaya, T Mizuno, I Terasaki, *Phys. Rev*. B **70** (2004) 092503.
56. Y Dagan, M M Qazilbash, C P Hill, V N Kulkarni and R L Greene, *Phys. Rev. Lett*. **92** (2004) 167001.
57. J E Sonier, K F Poon, G M Luke, P Kyriakou, R I Miller, R Liang, C R Wiebe, P Fournier and R L Greene, *Phys. Rev. Lett*. **91** (2003) 147002.
58. F Zamborszky, G Wu, J Shinagawa, W Yu, H Balci, R L Greene, W G Clark and S E Brown, *Phys. Rev. Lett*. **92** (2004) 047003.
59. O N Bakharev, I M Abu-Shiekah, H B Brom, A A Nugroho, I P McCulloch, J Zaanen, *Phys. Rev. Lett*. **93** (2004) 037002.
60. W Kohn, *Phys. Rev*. **133** (1964) A171.
61. E Dagotto, *Rev. Mod. Phys*. **66** (1994) 763 and references therein.
62. T Tohyama and S Maekawa, *Phys. Rev*. B **64** (2001) 212505.